Journal of Power Sources 220 (2012) 160–168

Contents lists available at SciVerse ScienceDirect

Journal of Power Sources

journal homepage: www.elsevier.com/locate/jpowsour

Carbon fabric-aligned carbon nanotube/MnO_2/conducting polymers ternary composite electrodes with high utilization and mass loading of MnO_2 for super-capacitors

Peng Lv, Yi Y. Feng, Yu Li, Wei Feng*

School of Materials Science and Engineering, Tianjin Key Laboratory of Composite and Functional Materials, Tianjin University, Tianjin 300072, China

HIGHLIGHTS

- Carbon fabric-aligned carbon nanotube (CF-ACNT) acted as a unique substrate.
- MnO_2 and poly(3,4-ethylenedioxythiophene) (PEDOT) were deposited on CF-ACNT.
- The ternary composites showed a high MnO_2 utilization of 77.7%.
- The 3D porous ternary system allowed large MnO_2 mass loading up to 3.11 mg cm^{-2}
- A reasonable area-normalized capacitance of 1.3 F cm^{-2} was achieved.

GRAPHICAL ABSTRACT

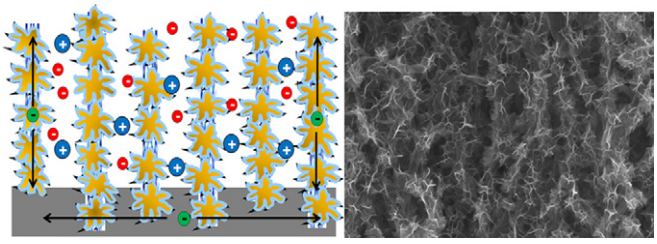

ARTICLE INFO

Article history:
Received 24 March 2012
Received in revised form
22 July 2012
Accepted 25 July 2012
Available online 4 August 2012

Keywords:
Aligned carbon nanotube
Carbon fabric
Manganese oxide
Poly(3,4-ethylenedioxythiophene)
Ternary composite
Super-capacitor

ABSTRACT

3D porous ternary composite electrodes have been prepared by electrodepositing MnO_2 and poly(3,4-ethylenedioxythiophene) (PEDOT) successively on carbon fabric-aligned carbon nanotube (CF-ACNT) hybrids for the super-capacitors. MnO_2 petal-like nano-sheets are deposited on the ACNT surface with PEDOT uniformly encapsulated and interconnected MnO_2 nano-sheets and ACNTs. Cyclic voltammetry shows the MnO_2 utilization of ternary composites up to 77.7%, which far exceeds that of MnO_2/CNT-based materials reported recently. Moreover, the 3D porous ternary system allows large mass loading of MnO_2. And the ternary composites can remain a high MnO_2 utilization of 36% with the MnO_2 mass loading up to 3.11 mg cm^{-2} while achieve a reasonable area-normalized capacitance of 1.3 F cm^{-2} at 0.1 mV s^{-1}. The ternary composites with substantially high mass loading exhibit an excellent rate capability and cycling stability, retaining over 95% of its initial charge after 1000 cycles. The excellent electrochemical performances are attributed to the synergetic effect of each component with unique properties and structures: high porosity and interconnectivity of CF, aligned ion diffusion channels along ACNTs, ultrathin MnO_2 nano-sheets and the improved conductivity by PEDOT.

1. Introduction

Super-capacitors or electrochemical capacitors have attracted much attention due to high power density, fast charging and discharging within seconds, superior cycle life time, and high reliability. A variety of materials with specific properties have been investigated to explore the great potential and applicability for advanced super-capacitors with high capacity performance, such as carbon-based materials, transition-metal oxides and conducting polymers [1–4]. However, previous attempts showed that the electrochemical properties of each material separately for super-

* Corresponding author. Fax: +86 22 87402059.
E-mail address: weifeng@tju.edu.cn (W. Feng).

0378-7753/$ – see front matter © 2012 Elsevier B.V. All rights reserved.
http://dx.doi.org/10.1016/j.jpowsour.2012.07.073

capacitors were limited by their intrinsic structural shortcomings. For example, although carbon nanotubes (CNTs) exhibit excellent properties including high conductivity, large surface area, good mechanical properties and chemical stability [5–7], CNT-based electrodes act only as a stable high-surface-area support without redox properties, thus showing relative low specific capacitance [8–10]. Conducting polymers have high flexibility, but the huge capacity loss during successive charge/discharge cycles restricts their application for super-capacitors [11,12]. In addition, MnO_2 as an important family member of transition-metal oxides is generally considered to be one of the most promising pseudocapacitive materials due to high theoretical specific capacitance, low cost, environmental friendliness and natural abundance [6,13,14]. Nevertheless, the electrochemical performances of MnO_2 are basically limited by poor electronic conductivity and dense morphology of the oxide [15,16].

To overcome the limitation of each potential material, the design of specific composites prepared by the complementary combination of highly pseudocapacitive MnO_2, conductive CNTs or flexible conducting polymers is regarded as a powerful candidate for outstanding electrode materials [17,18]. Based on this structure, many binary composites, such as MnO_2/CNT [19–23] and MnO_2/conducting polymers [24,25], have been studied for high electrochemical performances. However, MnO_2/conducting polymer composites suffer from the mechanical instability and poor cycleability [26,27]. In contrast, binary composites of MnO_2/CNT exhibit advanced electrochemical performances, such as high specific capacitance, enhanced electrical conductivity and good cycling stability, which are attributed to the improved conductivity and mechanical property by CNTs [28–30].

Despite great potential, the low utilization of MnO_2 at high mass loading is still a significant drawback of MnO_2/CNT binary composites. It is well known that the high transition-metal oxide concentration and large mass loading of active materials are essentially important for the high energy density of electrochemical applications [31]. However, dense morphology and poor conductivity of the binary composite electrodes due to high mass loading lead to the limited kinetics of charge transfer reaction and the difficulty in penetration of electrolyte into the bulk MnO_2 [30,32]. Thus, the challenge with MnO_2/CNT-based composites lies in maximizing their electrochemical utilization. The approaches considered to efficiently improve the utilization can be concluded to two kinds: assembly of ternary composites and formation of a 3D porous structure. On the basis of the former method, ternary composites of CNT/MnO_2/PEDOT-PSS [18,33], CNT-PSS/MnO_2/PPY [31,34] and CNT/MnO_2/PANI [35] have been prepared with the outstanding electrochemical properties due to a synergetic effect from the combination of three components. The contact resistance of the electrodes is minimized effectively by conducting polymers due to the good interparticle connectivity between MnO_2 and CNTs. In case of the later method, various carbon-based substrates, such as carbon nanofiber [36], carbon cloth [37,38], and CNT-textile [10,20] with a 3D porous network structure have been used for the controlled deposition of nano-structured MnO_2. The 3D porous architecture not only permits large loading of MnO_2 but facilitates easy access of electrolytes to the electrodes, resulting in high specific capacitance and good rate capability [39–41].

To further improve the electrochemical performances of MnO_2/CNT-based composite electrodes, especially the high utilization and mass loading of MnO_2, we intend to combine the two concepts to form a 3D porous ternary system, which should have large specific surface area (SSA), high porosity and low internal resistance. In the present work, the carbon fabric-aligned carbon nanotube (CF-ACNT) hybrids prepared by chemical vapor deposition (CVD) are used as a porous substrate for electrode materials. The CF-ACNT hybrids show high porosity, interconnected network, ordered porous structure and good electrical conductivity. The strategy of fabricating a 3D porous ternary composites is shown schematically in Fig. 1, where MnO_2 and poly(3,4-ethylenedioxythiophene) (PEDOT) are successively deposited on CF-ACNT hybrids. The electrochemical properties of the 3D porous ternary composites with specific nano-structure and synergetic effects are measured in comparison with those reported in previous studies.

2. Experimental

2.1. Preparation of CF-ACNT hybrids

The growth of ACNTs on CF was performed by CVD in a reactor corundum tube furnace. The furnace was firstly purged with 300 sccm argon and heated to 850 °C at 5 °C min^{-1}. A feeding solution of catalyst precursor (ferrocene, 0.025 g mL^{-1}) and hydrocarbon source (xylene:ethanol:ethylene diamine = 49:49:2) were injected to the chamber during 60 min growth by a syringe pump. By measuring the weight difference of CF with and without CNTs, the mass of about 1∼1.3 mg was obtained for CNTs on CF with a geometric surface area of about 1 cm^2.

2.2. Preparation of CF-ACNT/MnO_2 binary composites

MnO_2 was deposited onto CF-ACNT hybrids by a galvanostatic method with a three-electrode setup, where CF-ACNT, Pt foil and Ag/AgCl were used as working, counter and reference electrodes, respectively. A aqueous precursor solution with 0.1 M $Mn(CH_3COO)_2$ and 0.01M Na_2SO_4 was used as the electrolyte, and the deposition was performed at a constant current of 1 mA cm^{-2}. To ensure the conformal deposition of MnO_2 uniformly on CF-ACNT surface, the precursor solution was introduced into CF-ACNT hybrids by 10 min vacuum impregnation before the deposition. Typically, the area of the hybrids was 2 cm^2 and only 1 cm^2 was immersed in the electrolyte for deposition. A small piece of Pt was used to connect the hybrids and the alligator clip to avoid side reactions. After the deposition, the working electrodes were washed with distilled water and then dried under vacuum at 100 °C for 1 h. The MnO_2 mass loading was evaluated by calculating the weight difference of the working electrodes.

2.3. Preparation of CF-ACNT/MnO_2/PEDOT ternary composites

PEDOT was continuously deposited onto CF-ACNT/MnO_2 binary composites with the galvanostatic method as described in section 2.2. Aqueous solution consisting of 0.01 M EDOT and 0.005 M SDS was used for the deposition of PEDOT at a current of 0.5 mA cm^{-2}. And the pH value of aqueous solution was adjusted by slowly adding ρ-toluenesulfonic acid to pH = 1. The mass loading of the electrodes was evaluated same to section 2.2. The PEDOT was also deposited onto the CF-ACNT under the same condition for electrochemical comparison.

The composites were defined based on the various deposition time, for example, the composite of CF-ACNT/MnO_2(10)/PEODT(1) was prepared by the deposition of MnO_2 for 10 min and subsequently the deposition of PEDOT for 1 min. The details of the deposition time and weight fraction of different composites were presented in Table S1.

2.4. Material characterization

The chemical structure of composites was characterized by X-ray photoelectron spectroscopy (XPS), which was performed with a PHI 1600 spectroscopy using Mg kα X-ray source for excitation.

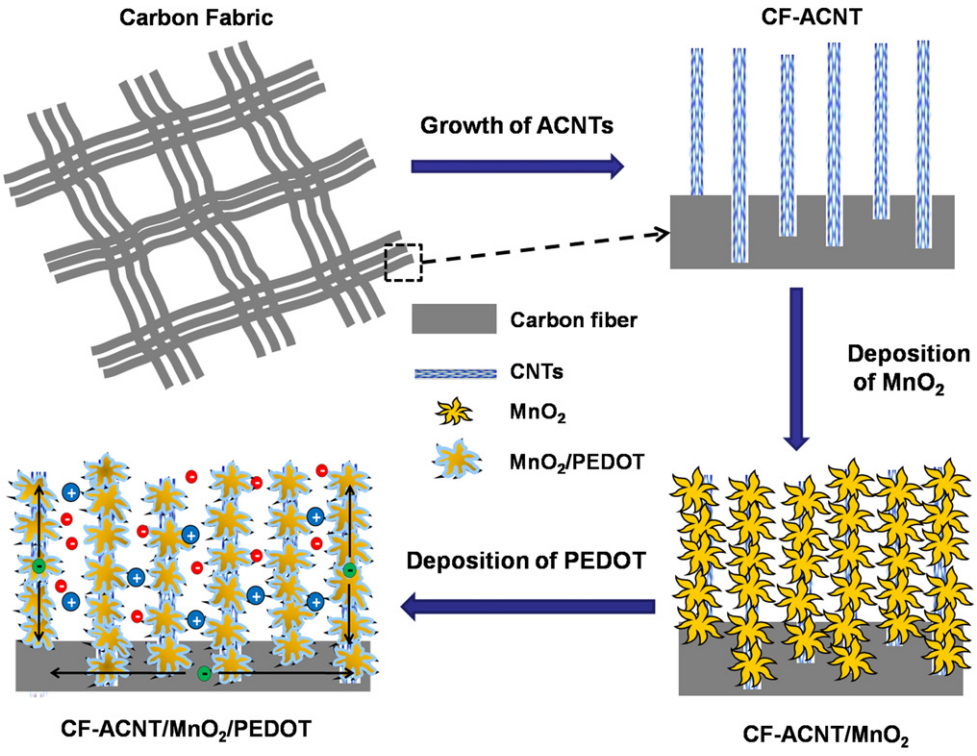

Fig. 1. Schematic illustration for the preparation of 3D porous ternary composites.

The crystal structure of the composites was characterized by Bruker D8 micro X-ray diffraction (XRD), operating at 40 kV and 40 mA, with Cu Ka radiation (k=0.15,418 nm). The nano-structures of CF-ACNT, CF-ACNT/MnO_2, and CF-ACNT/MnO_2/PEDOT were characterized by scanning electron microscopy (SEM) (Hatchi S-4800) operating at 15 KV and transmission electron microscopy (TEM) (FEI-Tecnai G2 F20) at 200 KV. The element composition of composites were determined by energy dispersive X-ray spectroscopy (EDX) equipped in TEM. Brunauer-Emmett-Teller (BET) surface area was measured by N_2 physisorption at 77K using a NOVA-2000 adsorption equipment.

2.5. Electrochemical measurement

The electrochemical characterization of the ternary composites was performed using a CHI660D electrochemical workstation (Shanghai CH Instrument Company, China) in Na_2SO_4 (1 M) solution. Ag/AgCl reference electrode and Pt counter electrode were used in the measurement. Cyclic voltammetry (CV) was carried out at different scan rates with a potential window from −0.1 ∼0.9 V. Galvanostatic charge/discharge tests were measured at a specific current of 1 A g^{-1}. The electrochemical impedance spectroscopy (EIS) measurements were conducted in the frequency from 100 kHz to 20 mHz with perturbation amplitude of 5 mV versus the open-circuit potential.

3. Results and discussion

X-ray photoelectron spectroscopy (XPS) was employed to study the chemical structure of composites. Fig. 2 shows the identical XPS spectra of the binary composites of CF-ACNT/MnO_2(10) and the ternary composites of CF-ACNT/MnO_2(10)/PEDOT(1). The presence of manganese oxide is evidenced by manganese Mn 3s and Mn 2p peaks along with oxygen O 1s peaks. The S 2p XPS transitions indicate that PEDOT has been deposited on the binary composite. As shown in Fig. 2b, the Mn 2p region consists of a spin-orbit doublet of Mn $2p_{1/2}$ with a binding energy of 653.8 eV and Mn $2p_{3/2}$ with a binding energy of 642.2 eV, which are characteristic of a mixed-valence manganese system [26]. Deconvoluted Mn $2p_{3/2}$ peaks at 642.6 and 641.8 eV are attributed to the presence of Mn^{4+} and Mn^{3+} oxide phases, respectively [42–44]. And the amount of Mn^{4+} and Mn^{3+} oxide phases is determined to be 73% and 27%, respectively, which indicates that the dominated oxidation state of manganese oxide in the composites is tetravalent oxide. The existence of Mn-oxide phases is also reflected in the O1s spectra shown in Fig. 2c. The spectrum can be deconvoluted into three constituents corresponding to Mn–O–Mn bond (529.6 eV) of the tetravalent oxide, Mn–O–H bond (531.4 eV) of a hydroxide, and H–O–H bond (532.7 eV) of residual water (Fig. 2c). Fig. 2d shows the XRD patterned of the CF-ACNT and CF-ACNT/MnO_2(10). The two characteristic peaks at 37.1° and 66.3° (marked by arrow) endorse the presence of MnO_2, which is consistent with the XPS analysis as mentioned above. The relative low-intensity and broad peaks suggest that MnO_2 is in amorphous nature, which is favorable for super-capacitor applications [45].

Morphologies of CF-ACNT hybrids, CF-ACNT/MnO_2(10) and CF-ACNT/MnO_2(10)/PEDOT(1) were observed by SEM. As shown in Fig. 3a, the vertical alignment of CNTs with the length of about 60 μm grown on CF forming a 3D porous configuration. In the inset of Fig. 3a, it can be seen that the ACNT array exhibits a regular pore structure and meso-porous size, which facilitates the intimate contact with electrolyte solution. As described in our previous report [46], the interface between CNTs and CF showed the CNT roots fastened on the surface of CF by embedded catalyst particles, leading to the direct contact and effective charge transport between CNTs and CF. SEM images of the CF-ACNT/MnO_2(10) are shown in Fig. 3b and c. It is clearly displayed that, after the deposition, reticular and curved petal-like nano-sheets are anchored on the

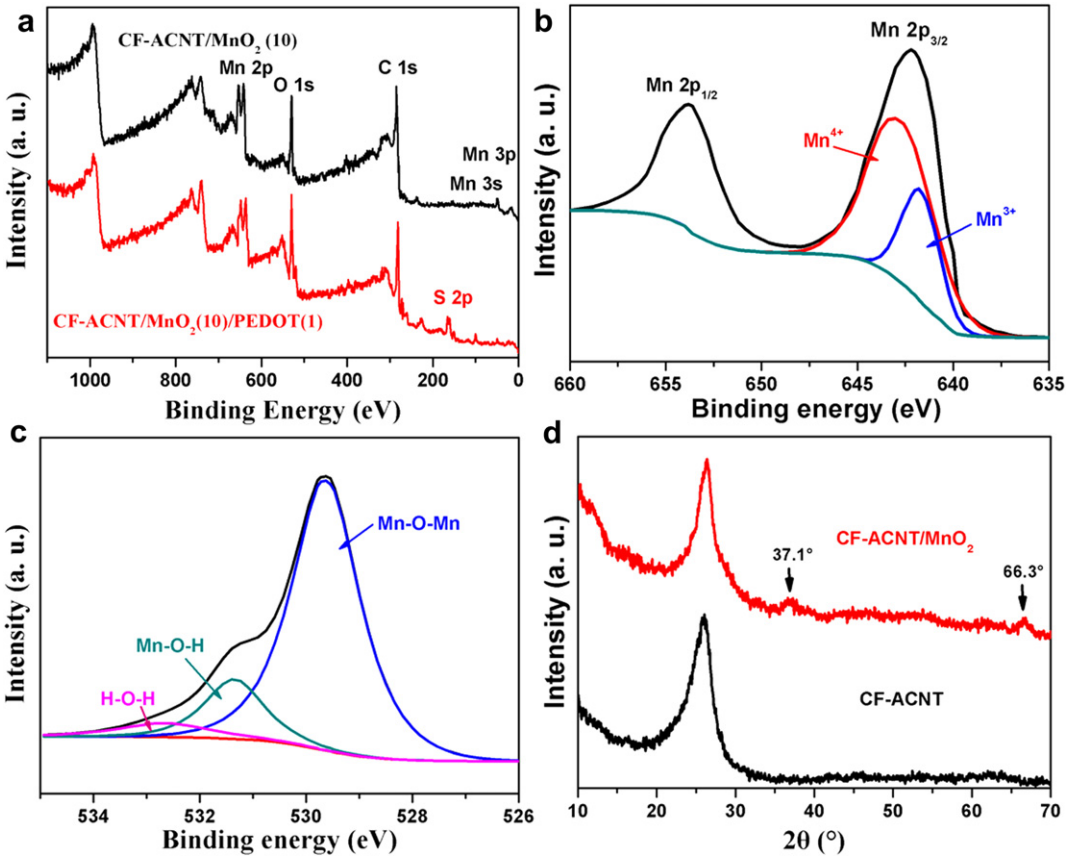

Fig. 2. (a) Surface scanning XPS spectra of CF-ACNT/MnO_2(10) and CF-ACNT/MnO_2(10)/PEDOT(1); (b) Mn 2p and (c) O1s core level XPS spectra with deconvoluted peaks for CF-ACNT/MnO_2(10)/PEDOT(1); (d) XRD patterns of CF-ACNT and CF-ACNT/MnO_2.

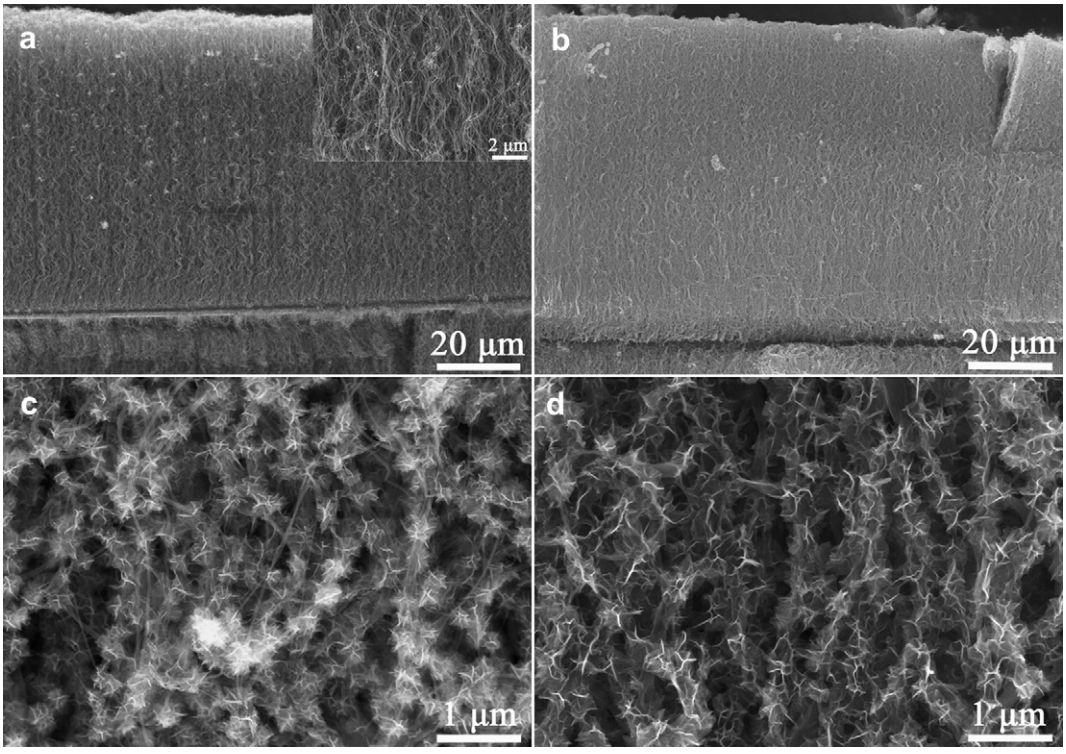

Fig. 3. SEM images of (a) CF-ACNT, (b, c) CF-ACNT/MnO_2(10) and (d) CF-ACNT/MnO_2(10)/PEDOT(1), respectively.

surface of the CNTs over the entire longitudinal length. The corresponding TEM image (Fig. 4a), revealing the inherent structure of the binary composites, shows that the transparent petal-like nano-sheets with a thickness of few nanometers and a width of about 70 nm are attached on the surface of the inner CNTs. The EDX-1 in Fig. 4d shows the resultant sample is composed of C, O and Mn elements, corroborating the petal-like nano-sheets are MnO_2. The uniform formation of MnO_2 deposited on the CNTs is attributed to the highly porous structure of CF-ACNT, where the interstitial voids enable the homogeneous penetration and fast flux of MnO_4^- ions into the interior substrate.

As shown in TEM images (Fig. 4b and c), the morphology of MnO_2 nano-sheets of the ternary composites is unchanged after the deposition of PEDOT, and a polymer layer with a thickness of nanometer is coated on both MnO_2 nano-sheets and CNTs. The EDX-2 in Fig. 4d indicates the existence of additional S element of the polymer layer ascribed to PEDOT phases. The SEM image (Fig. 3d) of the ternary composite shows that PEDOT uniformly covered the binary composite, interconnected MnO_2 nano-sheets and filled the interval between MnO_2 nano-sheets and CNTs. The deposition of PEDOT has little influence on the interface of MnO_2, due to no huge junks or aggregates are found in the composites. Different from the limited interaction between MnO_2 and CNTs in the binary composites, the ternary composites show a strong interaction with the intimate contact between MnO_2 nano-sheets and ACNT, which is beneficial for improving the stability of electrodes. In order to confirm the strong binding between each component, the ternary composite electrodes were flushed vigorously with water repeatedly and then no exfoliation or separation was observed. This feature is attributed to that PEDOT act as not only the additional electroactive material, but also the conductive binder.

BET surface area tests show the SSA of CF-ACNT, CF-ACNT/MnO_2(10) and CF-ACNT/MnO_2(10)/PEDOT(1) are 77, 237 and 203 $m^2\ g^{-1}$, respectively. The remarkable increase of the composites in the SSA compared to CF-ACNT arises from the surface coverage of MnO_2 hierarchical nano-sheets. And the SSA of the composites does not decrease dramatically after the PEDOT deposition. Such porous structure and high SSA provide high accessible area for electrolytic dopant ions from the electrolyte to the pseudo-capacitive materials.

CV was performed to evaluate the capacitive behavior of the composite electrodes. Fig. 5a shows the typical CV curves of CF-ACNT, CF-ACNT/PEDOT(1), CF-ACNT/MnO_2(10) and CF-ACNT/MnO_2(10)/PEDOT(1) electrodes at a scan rate of 5 mV s^{-1}. The CV response of CF-ACNT/MnO_2(10) is much larger than that of CF-ACNT and CF-ACNT/PEDOT(1), indicating that MnO_2 is mainly responsible for the high specific capacitance of the composites. Compared with CF-ACNT/MnO_2(10), CV curve of CF-ACNT/MnO_2(10)/PEDOT(1) is relatively rectangular in shape and exhibits

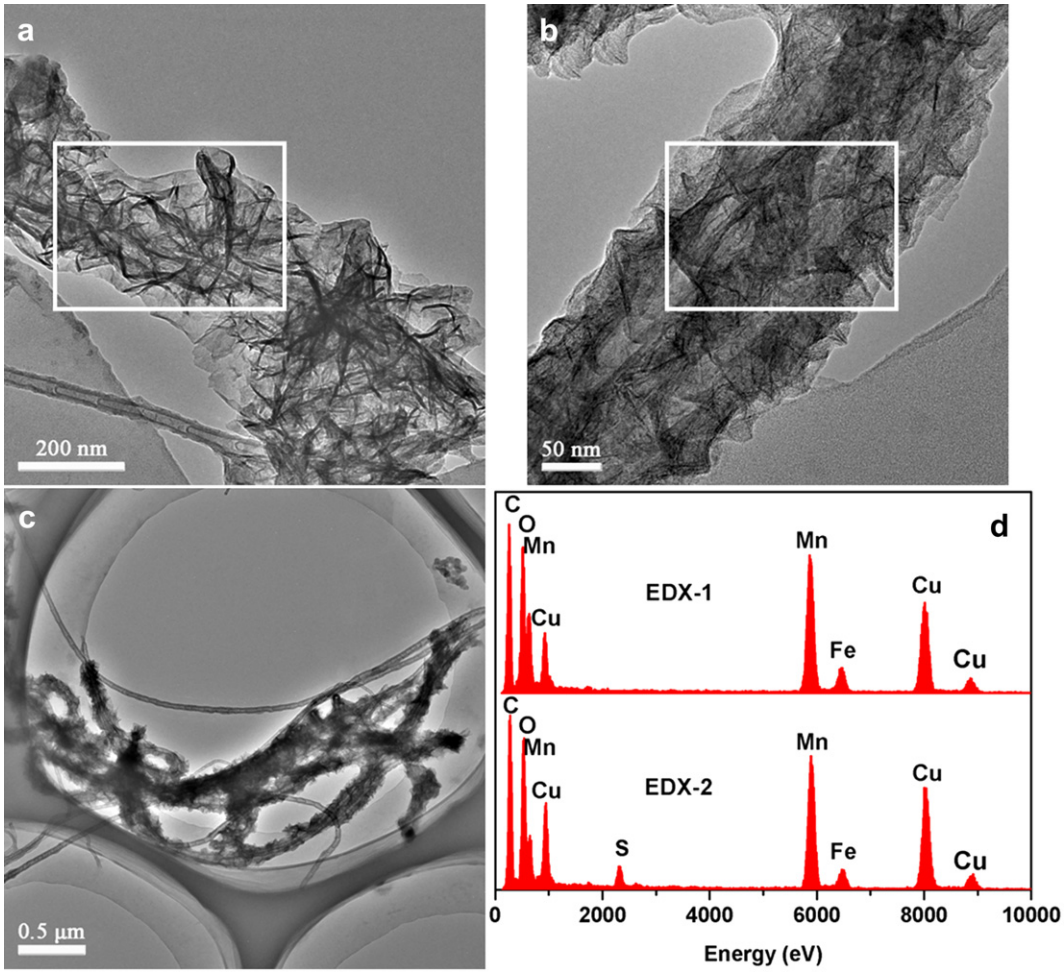

Fig. 4. TEM images of (a) CF-ACNT/MnO_2(10) and (b, c) CF-ACNT/MnO_2(10)/PEDOT(1); (d) EDX analysis on the square area marked in (a) and (b) corresponding to EDX-1 and EDX-2, respectively.

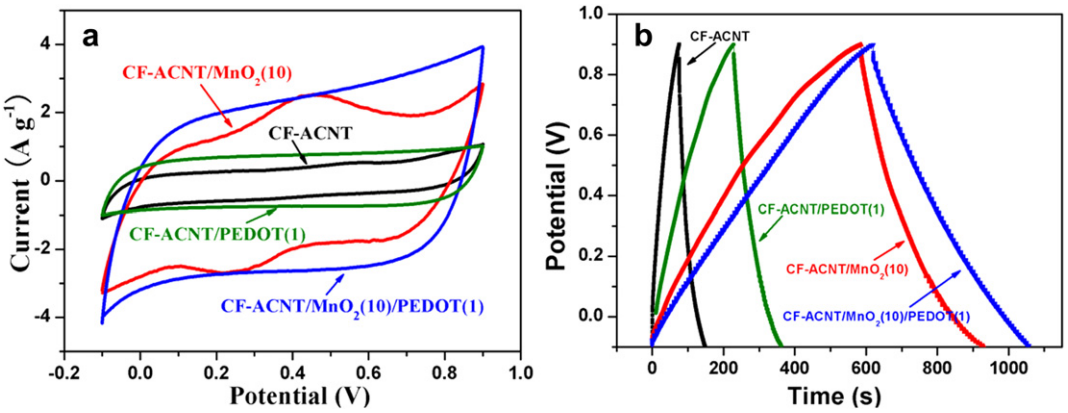

Fig. 5. (a) CV and (b) galvanostatical charge–discharge curves of CF-ACNT, CF-ACNT/PEDOT(1), CF-ACNT/MnO_2(10) and CF-ACNT/MnO_2(10)/PEDOT(1), respectively.

a mirror-like replication below and above the zero line. Calculation (see Supporting information) based on CV curves (Fig. 5a) indicates the specific capacitance C_{sp} values of CF-ACNT, CF-ACNT/PEDOT(1), CF-ACNT/MnO_2(10) and CF-ACNT/MnO_2(10)/PEDOT(1) are 71, 151, 404 and 481 F g^{-1}, respectively. In agreement with the CV results, the charge–discharging curves (Fig. 5b) of the composite electrodes show that the CF-ACNT/MnO_2(10)/PEDOT(1) exhibits a symmetrical and closely linear slope between −0.1 and 0.9 V at a specific current of 1 A g^{-1}.

Maximizing the utilization of MnO_2 is considered as a challenge because only MnO_2 on the surface can be utilized for charge storage. The comparison of MnO_2 utilization between this work and previous reports about MnO_2/CNT-based composites is shown in Table 1. Because of the contribution of CNTs and PEDOT to the total specific capacitance of composites is not negligible, the specific capacitance of MnO_2 component (C_{sp}(MnO_2)) in the composites can be estimated after subtracting the contribution of CNTs and PEDOT according to the following equation:

$$C_{sp}(\mathrm{MnO_2}) = \frac{C_{sp}(\mathrm{composite}) - C_{sp}(\mathrm{CNT/PEDOT}) \times \mathrm{wt\%(CNT/PEDOT)}}{\mathrm{wt\%(MnO_2)}} \quad (1)$$

where C_{sp} (composite) is the specific capacitance of the composites, C_{sp}(CNT/PEDOT) is the specific capacitance of the CF-CNTA/PEDOT prepared with the same deposition time to the corresponding 3D porous composites, wt%(CNT/PEDOT) and wt%(MnO_2) is the mass fraction of CNT/PEDOT and MnO_2 in the composites, respectively. And the MnO_2 utilization = C_{sp} (MnO_2)/1370 F g^{-1}. As shown in Table 1, a high MnO_2 utilization of CF-ACNT/MnO_2(10) up to 71.9% is achieved, which is higher than the values of MnO_2/CNT-based composites (typically<70%) in previous studies. The CF-ACNT/MnO_2(10)/PEDOT(1) with a utilization of 77.7% outperforms CF-ACNT/MnO_2(10) due to the controlled deposition of conductive PEDOT. It is noteworthy that the C_{sp} (MnO_2) reported in most of previous studies was calculated based on the mass of MnO_2 alone, without considering the contribution of the CNTs or conducting polymer to the specific capacitance of composites. This result indicates that the actual C_{sp}(MnO_2) is lower than the reported values. In addition, despite of relative costly nano-materials and complex methods, the MnO_2 utilization value (77.7%) of the present composite electrodes far exceeds that of the electrodes with low costly materials prepared by simple methods in previous studies (Table S2). Thus the 3D porous ternary composites can be developed as the promising electrode materials for high performance super-capacitors.

The high MnO_2 utilization can be attributed to the nano-structure and synergetic effects of the ternary composites. The porous ACNT arrays on the flexible CF provide much larger SSA than flat metal substrate [18,31,33,34], foam substrate [19] and CNT-textile fiber network [10,20] for loading MnO_2. In case of the same mass loading, the thickness of MnO_2 on CF-ACNT is much smaller than that of other substrates. Meanwhile, the ultrathin MnO_2 nano-sheets offer large electrochemically active surface areas for charge transfer and reduced ion diffusion length. However, CF-ACNT/MnO_2(10) still shows relatively distorted CV shape (Fig. 5a) and sluggish charge–discharge behaviors (Fig. 5b), indicating the high internal resistance, which inhibits charge transfer at the interface between MnO_2 and CNTs. According to previous works, the integration of conducting polymers into MnO_2/CNT-based composites is an efficient approach to improve the electrical conductivity [18,31,33,34]. As discussed above, the deposition of PEDOT can build an excellent conductive bridge across MnO_2 nano-sheets and CNTs facilitating charge transfer. The increase in conductivity of CF-ACNT/MnO_2(10)/PEDOT(1) was verified using EIS analysis. As shown in Fig. 6a, the Nyquist plot for the CF-ACNT/MnO_2(10) presents a high charge transfer resistance and a Warburg element of the diffusion limitation. In contrast, the Nyquist plots of the CF-ACNT/MnO_2(10)/PEDOT(1) suggest the significant decrease of the charge transfer resistance. Thus, the good combination of CF-ACNT, MnO_2 and PEDOT can maximize the MnO_2 utilization of the composites.

In order to further investigate the effect of PEDOT on the improvement of MnO_2 utilization, various deposition times of PEDOT were applied. As shown in Fig. 6b, the relationship between deposition time and C_{sp} values of the ternary composites at the scan rate of 5 mV s^{-1} suggests a optimum deposition time (1 min) for PEDOT to achieve high MnO_2 utilization. As shown in the SEM images of the ternary composites with 2 and 4 min deposition of PEDOT (Fig. 6c and d), the excessive loading of PEDOT results in aggregation and thick coating of PEDOT on MnO_2, which leads to the decrease of the interface area of MnO_2 for redox reaction.

Table 1
Comparison of the MnO_2 utilization of MnO_2/CNT-based composite electrodes. All values are measured using the three-electrode system.

No.	Composite	C_{sp} (MnO_2)	MnO_2 utilization	Condition	Ref.
1	CNT/MnO_2	471[a]	34.4%	10 mV s^{-1}	[28]
2	CNT/MnO_2	557[a]	40.7%	1 A g^{-1}	[36]
3	CNT/MnO_2	710[a]	51.8%	2 mV s^{-1}	[47]
4	ACNT/γ-MnO_2	784[a]	57.2%	1 mA cm^{-2}	[48]
5	CNT/MnO_2	869[a]	63.4%	2.5 A g^{-1}	[30]
6	CNT/MnO_2	944[a]	68.9%	1 mV s^{-1}	[19]
7	LbL-CNT/MnO_2	940[b]	68.6%	10 mV s^{-1}	[10]
8	CNT/polypyrrole/MnO_2	281[a]	20.5%	20 mV s^{-1}	[31]
9	CNT-PSS /polypyrrole/MnO_2	674[b]	49.2%	5 mV s^{-1}	[34]
10	CNT-PSS/PEDOT/MnO_2	781[a]	57%	5 mV s^{-1}	[18]
11	CF-ACNT/MnO_2(10)	985[b]	71.9%	5 mV s^{-1}	Present study
12	CF-ACNT/MnO_2(10)/PEDOT(1)	1065[b]	77.7%	5 mV s^{-1}	Present study

[a] C_{sp}(MnO_2) is calculated based on the mass of MnO_2 alone.
[b] C_{sp}(MnO_2) is calculated after subtracting the contribution of CNTs or CNT/conductive polymer.

The electrodes based on MnO_2 typically show a small mass loading (<0.5 mg cm^{-2}) due to its low proton diffusion constant and low conductivity [41]. The infinitely small thickness and low MnO_2 mass loading are basically acquired to achieve the high specific capacitance. However, the super-capacitors with high power performance ask for a high mass percentage of active materials with respect to the total mass of the device. Based on this requirement, the electrochemical properties of the ternary composites with high MnO_2 mass loading were studied. Fig. 7a shows the MnO_2 mass loading of ternary composites range from 0.71 to 3.79 mg cm^{-2} with the increase of MnO_2 deposition time. It can be seen in Fig. 7b, the CF-ACNT/MnO_2(35), corresponding to the mass loading of 3.11 mg cm^{-2}, still maintains the original petal-like shape of MnO_2 nano-sheets with high porosity. The SEM image of the CF-ACNT/MnO_2(35)/PEDOT(1) displays that, similar to the nano-structure of CF-ACNT/MnO_2(10)/PEDOT(1), PEDOT is uniformly deposited and interconnects MnO_2 nano-sheets and CNTs (Fig. 7c). However, when the deposition time of MnO_2 up to 40 min, the nano-sheets of MnO_2 begin to merge together, which influences the ion and electron transport within the electrodes (Fig. S1).

The C_{sp} values and MnO_2 utilization of the ternary composites with various MnO_2 mass loading measured by CV at 5 mV s^{-1} are shown in Fig. 7d. The C_{sp} values decrease from 481 to 374 F g^{-1} with the corresponding MnO_2 mass loading range from 0.71 to 3.11 mg cm^{-2}. However, the MnO_2 utilization still remains high value (36%) with a large mass loading of 3.11 mg cm^{-2}. As indicated in Fig. 7d, compare with others MnO_2/CNT-based materials reported in the studies [28,31,33,47], the 3D porous ternary system is appreciable as indicated by the high mass loading and reasonable utilization. It is worthy to point out that the mass loading of per area is also great important for high area-normalized capacitance. The area-normalized capacitances of the ternary composites with different MnO_2 mass loading were measured with a slow scan rate of 0.1 mV s^{-1} (Fig. S2). The composites with a mass loading of 3.11 mg cm^{-2} obtain the area-normalized capacitance of 1.3 F cm^{-2}, which is one or two orders higher than that of MnO_2/CNT materials reported previously (typically 0.01–0.1 F cm^{-2}) [10,36] and comparable to the best performance [41,49]. Although the area-normalized capacitance can reach higher values by the increase of MnO_2 deposition time, other electrochemical properties (such as specific capacitance, utilization and rate capability) decrease dramatically due to the extreme loading of MnO_2 and the dense morphology of composites (Fig. S2b).

The rate capability of the ternary composites was investigated over a wide range of scan rates from 5 to 200 mV s^{-1}. Fig. 8a shows the increase in current of the CF-ACNT/MnO_2(10)/PEDOT(1) with the increasing scan rates and no significant change of shape of CV

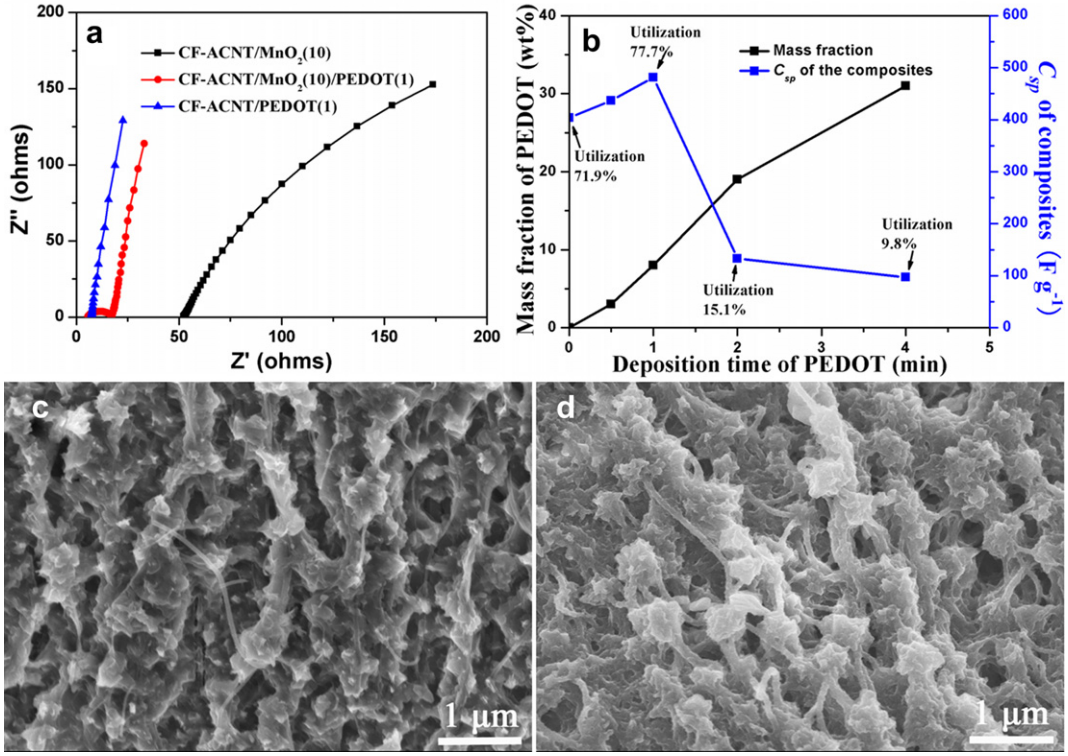

Fig. 6. (a) Nyquist impedance plots of CF-ACNT/MnO_2(10), CF-ACNT/MnO_2(10)/PEDOT(1) and CF-ACNT/PEDOT(1); (b) Mass fraction of PEDOT with the corresponding C_{sp} values and MnO_2 utilization for ternary composites as a function of the deposition time of PEDOT; SEM images of (c) CF-ACNT/MnO_2(10)/PEDOT(2) and (d) CF-ACNT/MnO_2(10)/PEDOT(4).

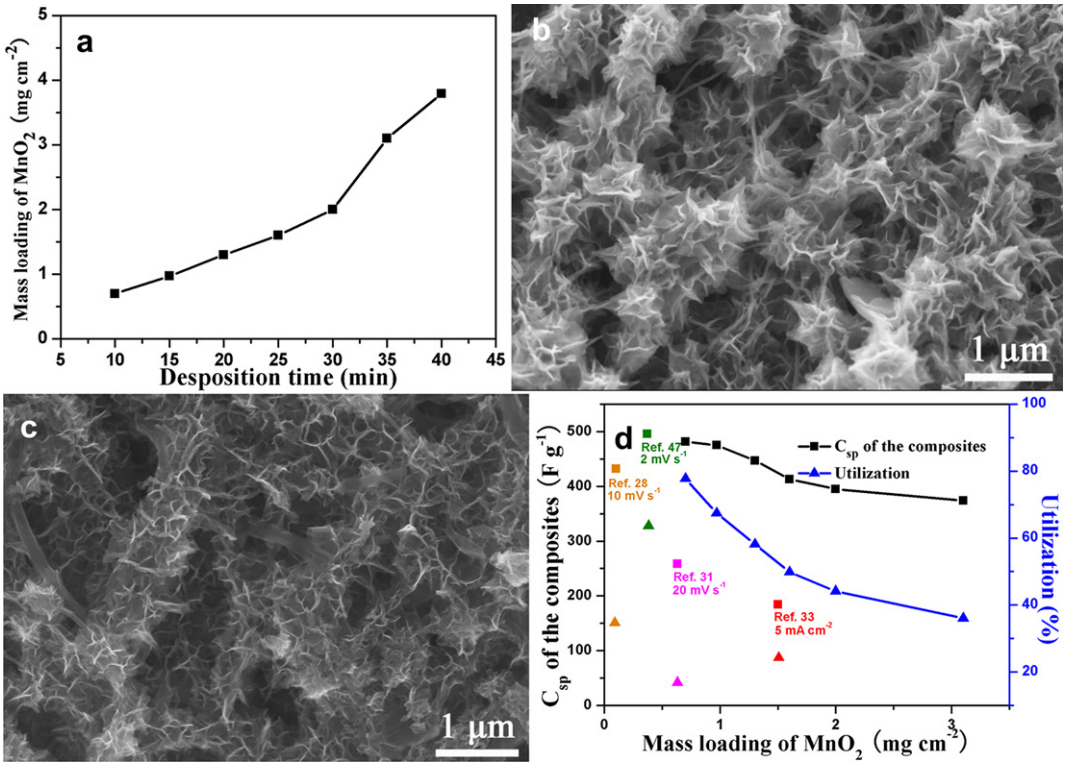

Fig. 7. (a) SEM images of CF-ACNT/MnO_2(35) and (b) CF-ACNT/MnO_2(35)/PEDOT(1); (c) MnO_2 mass loading as a function of the deposition time; (d) C_{sp} values of the ternary composites and their corresponding MnO_2 utilizations as a function of MnO_2 mass loading comparing with MnO_2/CNT-based composites reported in literatures (refs. [28,31,33,47]).

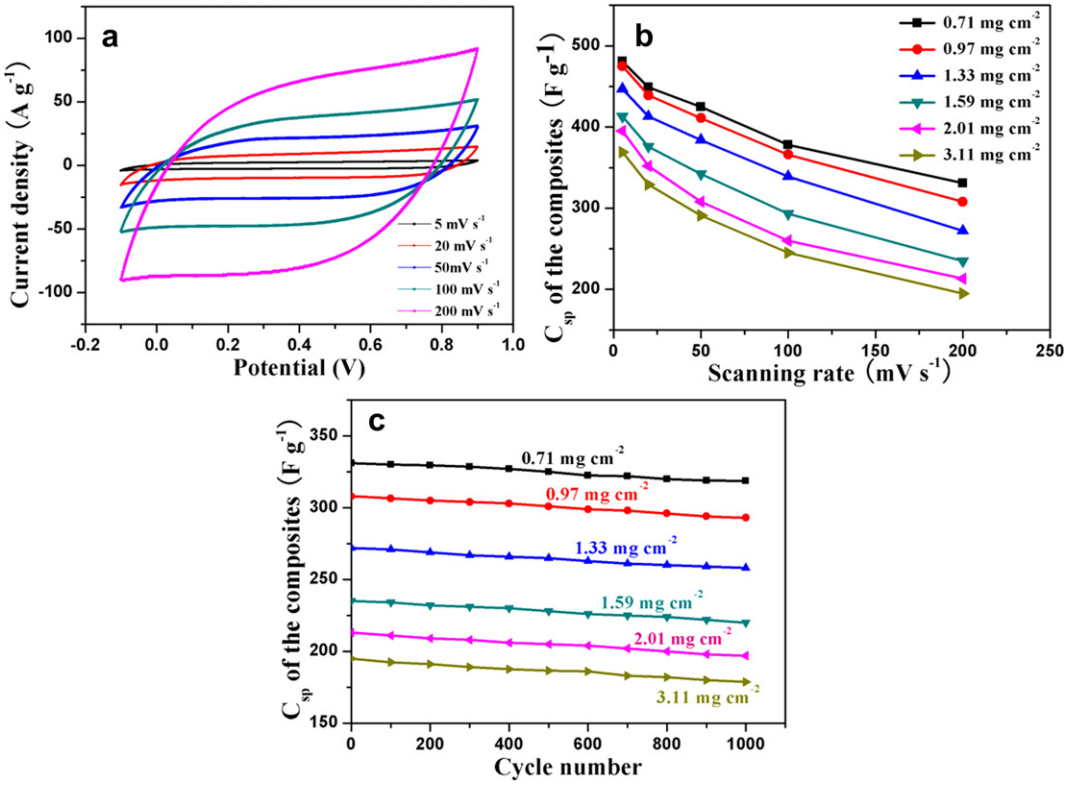

Fig. 8. (a) CV curves for CF-ACNT/MnO_2(10)/PEDOT(1) at various scan rates; (b) C_{sp} values of the ternary composites with different MnO_2 mass loading as a function of scan rates; (c) The variation of C_{sp} values stability of the ternary composites with cycle numbers.

curves at high rate. Fig. 8b shows that the C_{sp} value of CF-ACNT/MnO_2(10)/PEDOT(1) drops 31% at a high scan rate of 200 mV s^{-1} compared with that at low scan rate (5 mV s^{-1}). Moreover, the high MnO_2 mass loading does not result in the significant decrease in rate capability. The CF-ACNT/MnO_2(35)/PEDOT(1) with high MnO_2 mass loading of 3.11 mg cm^{-2} shows only a 50% loss of C_{sp} values with a scan rate ranging from 5 to 200 mV^{-1}(Fig. 8b). This performance outperforms others 3D porous systems, where the composites based on CNT or carbon nano-fiber textile, which show a drop of the specific capacitance about 77% [41] (5–200 mV s^{-1}), 60% [36] (2–100 mV s^{-1}) and 40% [40] (2–100 mV s^{-1}) with the MnO_2 mass loading of about 0.8, 0.33 and 0.25 mg cm^{-2}, respectively. This result indicates the ternary composites exhibit the comparable rate capacity with a substantially high mass loading, which is mainly attributed to the unique structure of the ternary composites: (1) the 3D porous nano-structure and the aligned channels of ACNT arrays favor fast electrolyte ion diffusion into the interior region of electrodes, (2) MnO_2 nano-sheets offer the large active surface area and the short diffusion paths for cations, (3) the good interfacial contact provides continuous conductive paths for electrons [48,50]. In addition, the cycle stability tests over 1000 CV cycles for the ternary composites were carried out at a scan rate of 200 mV s^{-1}. Fig. 8c shows the capacity loss of ternary composites less than 5% after 1000 consecutive cycles, suggesting that the synergetic interaction among CF-ACNT, MnO_2, and PEDOT significantly improved the electrical properties and the mechanical stability of electrodes.

4. Conclusion

CF-ACNT/MnO_2/PEDOT ternary composites with a 3D porous structure have been prepared by the electrochemical deposition for super-capacitors. The electrochemical characterization shows that the high MnO_2 utilization (77.7%) of ternary composite electrodes is achieved with the MnO_2 mass loading of 0.71 mg cm^{-2}. The utilization of ternary composites can maintain 36% with increasing the MnO_2 mass loading up to 3.11 mg cm^{-2}. Meanwhile the ternary composites with various mass loadings show high rate capacity and excellent cycling performance. Such excellent electrochemical properties are attributed to the nano-structure and synergetic effect of each component. CF-ACNT acts as a 3D framework with an interconnected porous structure, MnO_2 provides high charge storage ability and PEDOT serves as a conductive bridge. This 3D porous ternary system can be generalized toward other transition metal oxides, such as RuO_2, V_2O_5 and TiO_2 for high performance of super-capacitors.

Acknowledgements

This work was supported by the National Key Basic Research Program of China (Grant No. 2012CB626800 and 2010CB934700), and the National Natural Science Foundation of China (Grant Nos. 51073115, 51003072, 51173127, 51011140072), and Research Fund for the Doctoral Program of Higher Education of China (No.20110032110067).

Appendix A. Supplementary material

Supplementary data related to this article can be found online at http://dx.doi.org/10.1016/j.jpowsour.2012.07.073.

References

[1] J. Huang, B.G. Sumpter, V. Meunier, Angew. Chem. Int. Ed. 47 (2008) 520–524.
[2] M. Kaempgen, C.K. Chan, J. Ma, Y. Cui, G. Gruner, Nano Lett. 9 (2009) 1872–1876.
[3] D. Hulicova-Jurcakova, A.M. Puziy, O.I. Poddubnaya, F. Suarez-Garcia, J.M.D. Tascon, G.Q. Lu, J. Am. Chem. Soc. 131 (2009) 5026.
[4] C.C. Hu, K.H. Chang, M.C. Lin, Y.T. Wu, Nano Lett. 6 (2006) 2690–2695.
[5] C. Emmenegger, P. Mauron, P. Sudan, P. Wenger, V. Hermann, R. Gallay, A. Zuttel, J. Power Sources 124 (2003) 321–329.
[6] L. Hu, M. Pasta, F.L. Mantia, L. Cui, S. Jeong, H.D. Deshazer, J.W. Choi, S.M. Han, Y. Cui, Nano Lett. 10 (2010) 708–714.
[7] K.S. Raj, K. Ajay, S. Sudipta, Z. Lei, J. Power Sources 195 (2010) 1256–1262.
[8] C. Largeot, C. Portet, J. Chmiola, P.L. Taberna, Y. Gogotsi, P. Simon, J. Am. Chem. Soc. 130 (2008) 2730–2731.
[9] H.J. Zheng, W. Kang, F.M. Zhao, F.Q. Tang, T.E. Rufford, L.Z. Wang, C.N. Ma, Solid State Ionics 181 (2010) 1690–1696.
[10] S.W. Lee, J. Kim, S. Chen, P.T. Hammond, S.H. Yang, ACS Nano 4 (2010) 3889–3896.
[11] D.W. Wang, F. Li, M. Liu, G.Q. Lu, H.M. Cheng, Angew. Chem. 120 (2008) 379–382.
[12] D.W. Wang, F. Li, Z.G. Chen, G.Q. Lu, H.M. Cheng, Chem. Mater. 20 (2008) 7195–7200.
[13] Z.S. Wu, W. Ren, D.W. Wang, F. Li, B. Liu, H.M. Cheng, ACS Nano 4 (2010) 5835–5842.
[14] S. Chen, J. Zhu, X. Wu, Q. Han, X. Wang, ACS Nano 4 (2010) 2822–2830.
[15] X.H. Tang, Z.H. Liu, C.X. Zhang, Z.P. Yang, Z.L. Wang, J. Power Sources 193 (2009) 939–943.
[16] S.B. Ma, K.W. Nam, W.S. Yoon, X.Q. Yang, K.Y. Ahn, K.H. Oh, K.B. Kim, J. Power Sources 178 (2008) 483–489.
[17] K. Okamura, R. Inoue, T. Sebille, K. Tomono, M. Nakayama, J. Electrochem. Soc. 158 (2011) A711–A717.
[18] R.K. Sharma, L. Zhai, Electrochim. Acta 54 (2009) 7148–7155.
[19] J. Yan, Z.J. Fan, T. Wei, J. Cheng, B. Shao, K. Wang, L.P. Song, M.L. Zhang, J. Power Sources 194 (2009) 1202–1207.
[20] J.H. Kim, K.H. Lee, L.J. Overzet, G.S. Lee, Nano Lett. 11 (2011) 2611–2617.
[21] H. Zhang, G. Cao, Z. Wang, Y. Yang, Z. Shi, Z. Gu, Nano Lett. 8 (2008) 2664–2668.
[22] H.J. Zheng, F.Q. Tang, Y. Jia, L.Z. Wang, Y.C. Chen, M. Lim, L. Zhang, G.Q. Lu, Carbon 47 (2009) 1534–1542.
[23] S.W. Lee, J. Kim, S. Chen, P.T. Hammond, Y.S. Horn, ACS Nano 4 (2010) 3889–3896.
[24] R. Liu, S.B. Lee, J. Am. Chem. Soc. 130 (2008) 2942–2943.
[25] R. Liu, J. Duay, S.S. Lee, ACS Nano 4 (2010) 4299–4370.
[26] F.J. Liu, J. Power Sources 182 (2008) 383–388.
[27] Q. Lu, Y.K. Zhou, J. Power Sources 196 (2011) 4088–4094.
[28] K.W. Nam, C.W. Lee, X.Q. Yang, B.W. Cho, W.S. Yoon, K.B. Kim, J. Power Sources 188 (2009) 323–331.
[29] R.R. Jiang, T. Huang, Y. Tang, J.L. Liu, L.G. Xue, J.H. Zhuang, A.S. Yu, Elctrochim. Acta 54 (2009) 7173–7179.
[30] T. Bordjiba, D. Belanger, Electrochim. Acta 55 (2010) 3428–3433.
[31] S.R. Sivakkumar, J.M. Ko, D.Y. Kim, B.C. Kim, G.G. Wallace, Electrochim. Acta 52 (2007) 7377–7385.
[32] F. Teng, S. Santhanagopalan, Y. Wang, D.D. Meng, J. Alloys Compd 499 (2010) 259–264.
[33] Y. Hou, Y.W. Cheng, T. Hobson, J. Liu, Nano Lett. 10 (2010) 2727–2733.
[34] R.K. Sharma, A. Karakoti, S. Seal, Z. Lei, J. Power Sources 195 (2010) 1256–1262.
[35] Q. Li, J. Liu, J. Zou, A. Chunder, Y. Chen, L. Zhai, J. Power Sources 196 (2011) 565–572.
[36] J.G. Wang, Y. Yang, Z.H. Huang, F. Kang, Electrochim. Acta 56 (2011) 9240–9247.
[37] Y.C. Chen, Y.K. Hsu, Y.G. Lin, Y.K. Lin, Y.Y. Horng, L.C. Chen, K.H. Chen, Electrochim. Acta 56 (2011) 7124–7130.
[38] M.S. Wu, Z.S. Guo, J.J. Jow, J. Phys. Chem. C 114 (2010) 21861–21867.
[39] X.W. Cui, F.P. Hu, W.F. Wei, W.X. Chen, Carbon 49 (2011) 1225–1234.
[40] G.H. Yu, L.B. Hu, M. Vosgueritchian, H.L. Wang, X. Xie, J.R. McDonough, X. Cui, Y. Cui, Z.N. Bao, Nano Lett 11 (2011) 2905–2911.
[41] L.B. Hu, W. Chen, X. Xie, N. Liu, Y. Yang, H. Wu, Y. Yao, M. Pasta, H.N. Alshareef, Y. Cui, ACS Nano 5 (2011) 8904–8913.
[42] W. Xiao, D. Hu, C. Peng, G.Z. Chen, ACS Appl. Mater. Interfaces 3 (2011) 3120–3129.
[43] H.W. Nesbitt, D. Banerjee, Am. Mineral 83 (1998) 305–315.
[44] V.D. Castro, G. Polzonetti, J. Electron. Spectrosc. Relat. Phenom. 48 (1989) 117–123.
[45] S.J. Bao, B.L. He, Y.Y. Liang, W.J. Zhou, H.L. Li, Mater. Sci. Eng. A 397 (2005) 305–309.
[46] P. Lv, Y.Y. Feng, P. Zhang, H.M. Chen, N.Q. Zhao, W. Feng, Carbon 49 (2011) 4665–4673.
[47] Y.J. Kang, B. Kim, H. Chung, W. Kim, Synth. Met. 160 (2010) 2510–2514.
[48] Z. Fan, J.H. Chen, B. Zhang, B. Liu, X.X. Zhong, Y.F. Kuang, Diamond Relat. Mater. 17 (2008) 1943–1948.
[49] X. Jin, W. Zhou, S. Zhang, G.Z. Chen, Small 3 (2007) 1513–1517.
[50] C.C. Liu, D.S. Tsai, W.H. Chung, K.W. Li, K.Y. Lee, Y.S. Huang, J. Power Sources 196 (2011) 5761–5768.